Hindawi
Journal of Nanomaterials
Volume 2023, Article ID 2855788, 8 pages
https://doi.org/10.1155/2023/2855788

Research Article

Antiproliferative Activity of PEG-PEI-SWCNTs against AMJ13 Breast Cancer Cells

Marwa R. Jwameer,[1] Sabah A. Salman,[1] Farah T. M. Noori,[2] Ghassan M. Sulaiman,[3] Majid S. Jabir,[3] Khalil A. A. Khalil,[4,5] Elsadig M. Ahmed,[4,6] and Mohamed T. A. Soliman[4]

[1]*Department of Physics, College of Science, University of Diyala, Diyala, Iraq*
[2]*Department of Physics, College of Science, University of Baghdad, Baghdad, Iraq*
[3]*Division of Biotechnology, Department of Applied Sciences, University of Technology, Baghdad, Iraq*
[4]*Department of Medical Laboratories, College of Applied Medical Sciences, University of Bisha, P.O. Box 551, Bisha 61922, Saudi Arabia*
[5]*Department of Medical Laboratory Sciences, Faculty of Medicine and Health Sciences, Hodeidah University, Al Hudaydah, Yemen*
[6]*Department of Clinical Chemistry, Faculty of Medical Laboratory Sciences, University of El Imam El Mahdi, P.O. Box 27711, Kosti 209, Sudan*

Correspondence should be addressed to Ghassan M. Sulaiman; ghassan.m.sulaiman@uotechnology.edu.iq and Majid S. Jabir; 100131@uotechnology.edu.iq

Received 23 September 2022; Revised 9 January 2023; Accepted 21 January 2023; Published 8 February 2023

Academic Editor: Kondareddy Cherukula

Single-walled carbon nanotubes (SWCNTs) involving polyethylene glycol (PEG) and polyethyleneimine (PEI), which contain amines, were produced and analyzed using X-ray diffraction (XRD), UV–vis spectroscopy, Raman spectroscopy (RS), and transmission electron microscopy (TEM) for the spectral and structural analyses of PEG-PEI-SWCNTs. PEG-PEI-SWCNTs demonstrated peaks using UV–vis spectroscopy at 300.98 nm, have a broad peak at $2\theta = 23.51$, linked to 002 with d-spacing (3.7816), and have crystalline sizes of 8.48 nm. In PEG-PEI-SWCNTs, TEM images demonstrated the accumulation of SWCNTs with PEG-PEI due to an increased main grain size with functionalization to 80.68 nm. The D and G bands in PEG-PEI-SWCNTs moved to 1,292 and 1,586 cm^{-1}, respectively. SWCNTs are observed as a bundle of inhomogeneous, long-curved accumulates containing multitudes of tubes. The PEG-PEI-SWCNTs have a tubular structure that demonstrates particles scattered alongside the carbon nanotube sidewalls, which indicate that PEG and PEI are conjugated to the SWCNTs. Cytotoxicity evaluation of PEG-PEI-SWCNTs (6.25–100 μg/mL) in the breast cancer AMJ13 cell line was conducted for 24 and 72 hr, and the results showed enhanced toxicity to the tumor cells and decreased cytotoxicity against rhabdomyosarcoma (RD) normal cells.

1. Introduction

Single-walled carbon nanotubes (SWCNTs), a novel polyaromatic chemical, are researched for probable drug delivery because of their ultrahigh surface zones; high mechanical strength and physical elasticity; and electrical, chemical, and thermal stability [1]. SWCNTs have shown their role in intracellular drug transport, diagnostic imaging agents, and treating tumor cells [2]. SWCNTs may be able to cross a variety of cellular barriers while also carrying a substantial payload of the agent to be administered [3]. Moreover, the inherent spectroscopic characteristics of nanotubes, such as Raman shift and photoluminescence, enable the tracking, detection, and imaging of their transporting drugs [3]. Additionally, they can alter the chemoresistance process in tumor cells [4]. PEGylation (i.e., functionalization of carbon nanotubes with polyethylene glycol (PEG) moieties) is used to enhance the aqueous solubility, stability, and biocompatibility of CNT conjugates. Additionally, the PEG's "stealth" ability aids in prolonging blood circulation time and overcoming the

phagocytic activity of the reticuloendothelial system. The template for modification, such as the conjugation of ligands to physiological targets, is provided via PEGylation as well [5]. Despite having a wide range of pharmacological applications, polyethyleneimine (PEI), an aqueous-soluble cationic polymer (molecular weight (MW) 600–60,000 Daltons (Da)), is constrained by its MW, charge density, structure, and conformational flexibility [6]. Previous studies have demonstrated that PEGylation of PEI can improve particle dispersion at high concentrations, prevent particle aggregation, prolong blood circulation, and reduce systemic toxicity [7, 8]. We, therefore, developed SWCNTs for drug administration, employing PEG-PEI-SWCNTs as hydrophilic biocompatible block copolymers. SWCNTs and PEG-PEI are coupled, increasing the ester contact between them. Subsequently, this relationship was described via X-ray diffraction (XRD), UV–vis spectroscopy, Raman spectroscopy (RS), and transmission electron microscopy (TEM).

2. Experimental Setup

2.1. Preparation of PEG 4000–PEI-Functionalized SWCNTs. On the electromagnetic mixer, 0.4 g of SWCNTs (99%, 32%, Sigma–Aldrich) was stirred in a 1 : 1 solution of sulfuric and nitric acid for 2 hr without heat. After 2 hr of mixing, the product was filtered through filter paper, rinsed with ionic water and methanol, and then precipitated to produce the powder. Afterward, 120 mL of ionic water was added into different beakers, 6.2 g of EDC-HCl and 3.5 g of N-hydroxysuccinimide (NHS) (98.00%, Sigma-Aldrich) were added, and the electromagnetic mixer was set for 30 min to dissolve the substance in the ionic water; after half an hour, SWCNTs were added at this stage (SWCNTs–COOH). The solution was added into a Petri dish and placed in an electric oven at a temperature of 80°C to dry after adding 96 g of PEG 4000 (HiMedia, USA) and 8 g of PEI (Sigma–Aldrich) progressively and turning on the electromagnetic mixer for 24 hr. A paste-like substance with a sticky texture that was obtained signified high viscosity and was stored in a glass box for later use.

2.2. Characterization of PEG 4000–PEI-Functionalized SWCNTs. By measuring the solution's absorption spectrum using a UV–vis spectroscopy (UV–vis, Seoul, Korea) in the range of 225–500 nm, PEG 4000–PEI-functionalized SWCNTs were obtained. Rotational, vibrational, and low-frequency modes were examined using RS. To identify molecules, RS was used to analyze their structural fingerprint. To measure the samples, a 532 nm line, an argon laser, incident laser strength (5 mW), and automatic software switching of excitation wavelength with intensity calculation (Bruker Senterra Raman microscope) were used. To confirm the crystal structure (crystal phases and crystallite size) of the produced NPs, XRD analysis was carried out using the XRD-6000, Shimadzu, Japan. The crystallite size (D) of nanoparticles (NPs) and their conjugates were calculated using Scherrer equation (Equation (1)):

$$D = \frac{K\lambda}{\beta \cos\theta}, \tag{1}$$

where λ is the wavelength of X-rays, β is the full width at half maximum of the diffraction peak, and θ is Bragg's angle. In this study, the system was supplied with Cu Kα radiation with a wavelength (λ) of 1.5406 nm produced at 40 kV. To determine the morphological features of NPs, TEM (Zeiss, Germany) was used. The infrared (IR) transmission spectra were recorded by double-beam Fourier transform infrared (FTIR) spectroscopy using an IRAffinity-1 Shimadzu spectrophotometer (Columbia, MD, USA). The technique operates in the wavenumber range of 4,000–400 cm^{-1} with a resolution of 0.5 cm^{-1}. Atomic force microscopy (AFM) was measured by an SPM-AA3000 contact mode spectrometer (Angstrom Advanced Inc., USA). This test relies on producing an electron beam with high energy to be passed through the targets to investigate the material's microstructure.

2.3. Bioactivity of PEG-PEI-SWCNTs

2.3.1. Cell Culture. Human breast cancer AMJ13 cells and human rhabdomyosarcoma (RD) cells were cultured in tissue culture flasks (T 25 cm^2; Falcon, USA) containing RPMI-1640 medium (Capricorn, Germany), supplemented with 10% fetal bovine serum (Capricorn, Germany), penicillin (100 units/mL), and streptomycin (100 g/mL) [9, 10].

2.3.2. Cytotoxicity Assays. For PEG-PEI-SWCNTs, the cytotoxicity was evaluated in 96-well plates using the 3-(4,5-dimethylthiazol-2-yl)-2,5-diphenyl-2H-tetrazolium bromide (MTT) test (BioWorld, USA). The cell lines (1×10^4 cells/well) were incubated for 24 hr, followed by treatment with various doses (6.25–100 μg/mL) of PEG-PEI-SWCNTs [11]. After 24 and 72 hr of incubation, MTT (2 mg/mL) solution was added for 3 hr at 37°C, followed by washing and treatment with dimethyl sulfoxide (DMSO) (Santa Cruz, USA). The experiment was performed in triplicates, and the assay was read at 492 nm. The cytotoxicity (%) was evaluated using Equation (2) [12, 13]:

$$\text{Cytotoxicity } (\%) = A - \frac{B}{A \times 100}, \tag{2}$$

where A and B are the optical densities of controls and samples, respectively.

For cell morphology visualization, the cells were incubated in 24-well microtitration plates (1×10^5 cells/mL) for 24 hr at 37°C [14], followed by 24 hr incubation with PEG-PEI-SWCNTs at IC_{50}. At the end of incubation, cells were stained with crystal violet dye for 10–15 min [15, 16], followed by washing, and images were obtained after visualization under an inverted microscope (40×) [17, 18].

2.3.3. Statistical Analysis. To statistically analyze the data, GraphPad Prism 8 and the unpaired t-test were used. The results were calculated using the average standard deviation of three different measurements [19, 20].

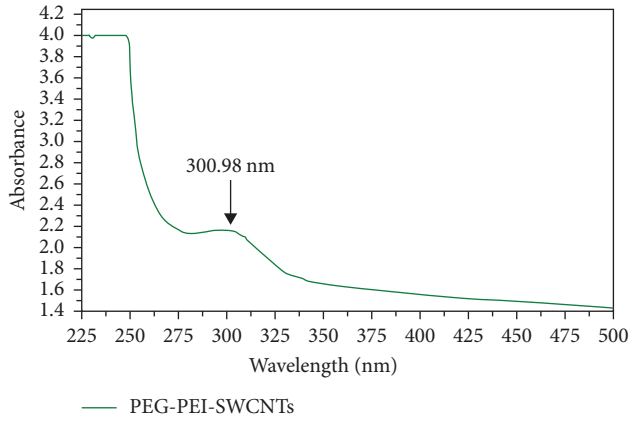

Figure 1: UV–vis absorption spectra of PEG-PEI-SWCNTs. The peak is located at 300.98 nm.

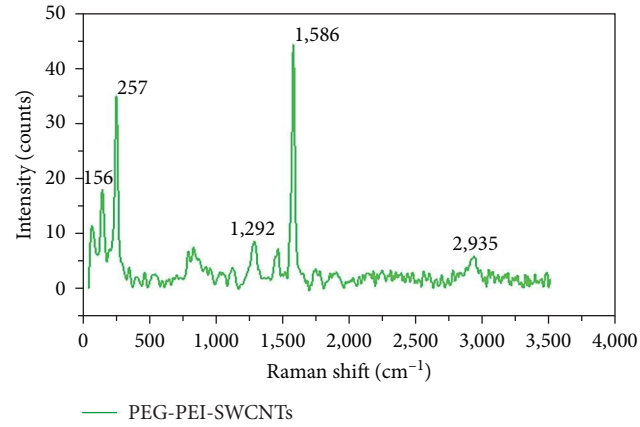

Figure 2: Raman spectra of functionalized PEG-PEI-SWCNTs. It represents D, G, and RBM bands.

3. Results and Discussion

3.1. Physical Characterization of PEG-PEI-SWCNTs. PEGylation (PEG-PEI-SWCNTs) was determined using UV–vis spectroscopy, XRD, RS, and TEM. Figure 1 shows the synthesized PEG-PEI-SWCNTs' structural bonding scheme.

3.1.1. UV–Vis Analysis. The green line, as shown in Figure 1, shows the spectra of PEG-PEI-SWCNTs at 300.98 nm and SWCNTs at 289 nm, which were obtained using UV–vis spectroscopy. These results were reported in a study by Jwameer et al. [21], which are absorption bands caused by electrons' movement π–π^* from C–C (aromatic rings) to n–π^* for C=O for SWCNTs. Green line shifting indicates PEG-PEI-SWCNTs synthesis [22, 23].

3.1.2. Raman Spectroscopy. Figure 2 depicts the Raman spectra of SWCNTs-PEG. SWCNTs' spectrum shows the following: (1) vibration of all atoms in phase termed as radial breathing mode (RBM) band (150.89 and 255.91 cm^{-1}); (2) disorder or D band (1,291.60 cm^{-1}), coupled to sp^2 carbon atoms breathing actions in the rings that become activated due to nanotube surface defects; (3) the tangential mode or G band (1,572.65 cm^{-1}), encompassing subbands G+ and G−, which correspond to axial and circumferential in-plane pulsations in semiconducting nanotubes, respectively; and (4) D or 2D bands of overtone (2D band), which are the graphitic assembly's impression, are seen at 2.566 cm^{-1}. The D and G bands' intensity disparities and width modification depict functionalization extents that are estimated due to the occurrence of organic fragments on the CNTs' sidewalls; this result has been published in the study [21]. The Raman spectra of PEG-PEI-SWCNTs are shown in Figure 2, where 1,292, 1,586, 156, and 257 cm^{-1} denote the D band, G band, and RBM, respectively. The ID/IG band intensity ratios provide a quantitative estimate of the functionalization extent. The ID/IG ratio of SWCNT is 0.82 before adding PEG-PEI-SWCNTs but decreases to 0.81 after absorbing PEG-PEI-SWCNTs. This trend indicates a weakening of Raman activity in the case of functionalized materials. We estimated an ID/IG ratio based on the fitting method, which decreases as one progresses from pure SWCNTs to functionalized materials. The G band is likewise expanding as a result of this tendency. This increase is due to a breach in the symmetry of the graphene sheet, due to functionality priming on the nanotube's surface, and is consistent with previous PEGylated–PEI systems [24]. To determine the nanotube's diameter since its frequency is inversely proportional to the reciprocal of the diameter, RBM may be used. The RBM also offers information on chirality and, consequently, on the nanotube's electrical characteristics. Because our experiment only used a single excitation energy, only nanotubes resonant with that energy will show a peak at the RBM frequency. $V_{\mathrm{RBM}} = 248/\omega$ [25], where V_{RBM} is the Raman frequency shift of the RBM (in cm^{-1}), may be used to calculate the nanotube's diameter. The estimated SWCNT diameter is based on the observed RBM (1.27) [26].

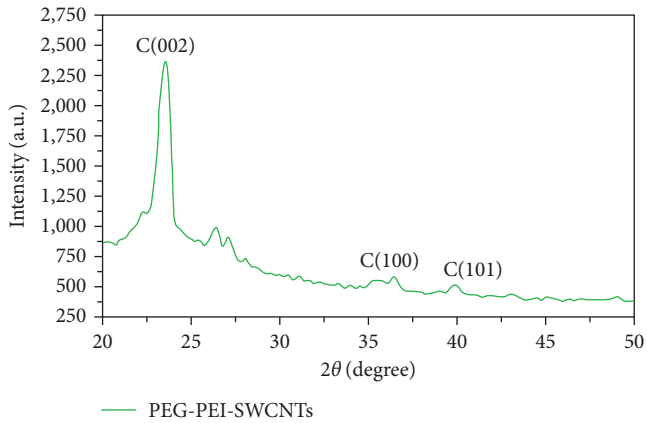

Figure 3: XRD patterns for PEG-PEI-SWCNTs. It was synthesized using an organic chemical method. A sharper peak was recorded at $2\theta = 23.51$. The diffraction patterns of the SWCNTs remain the same after conjugation with PEG and PEI.

3.1.3. X-Ray Diffraction. The green line, as shown in Figure 3, shows the XRD of PEG-PEI-SWCNTs with broad peaks ($2\theta = 23.51$) and d-spacing (3.7816). PEG-PEI-SWCNTs disrupted the crystallization order, which resulted in decreased PEG crystallinity and paved the way for effective ester bonding

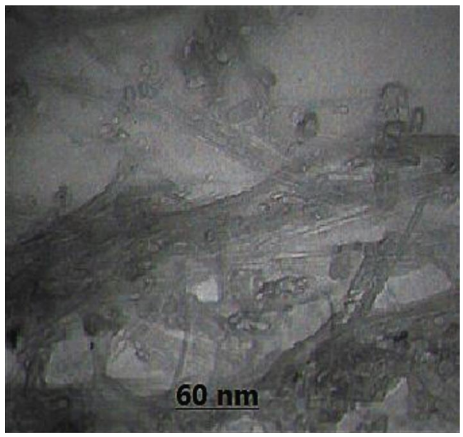

Figure 4: TEM images of PEG-PEI-SWCNTs with a rough tubular structure. Some particles appeared to be attached and distributed along the SWCNT sidewalls, indicating that PEG and PEI are conjugated onto nanotube. Scale bar: 60 nm.

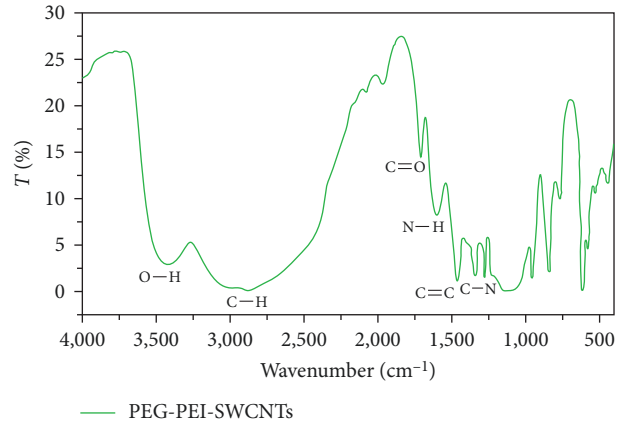

Figure 5: FTIR spectrum of functionalized PEG-PEI-SWCNTs. It shows the appearance of C=C, C–N, C=O, and N–H, demonstrating the successful conjugation of amino groups onto the surface of PEG-PEI-SWCNTs.

of PEG-PEI-SWCNTs [27]. The orientation (002), with 8.48 nm for PEG-PEI-SWCNT's crystalline size, was determined using the HighScore Plus program.

3.1.4. Morphological Properties of PEG-PEI-SWCNTs. To examine the morphology of PEG-PEI-SWCNTs, the truncated and functionalized TEM images were employed (Figure 4). Shorter SWCNTs that have been acid-treated had a smaller tube dimension and a hollow lumen tubular structure that are ideal for nanotube endocytosis. CNTs–COOH disperses into single tubes with smooth surfaces, no accumulation, and uniform morphological properties when produced with various acids. The PEG-PEI-SWCNTs have a rough tubular form scattered across SWCNT sidewalls, validating their conjugation with PEG and PEI (Figure 4).

3.1.5. FTIR Analysis. In FTIR spectra of SWCNTs, the stretching peaks at 3,431 cm^{-1} were assigned for the OH group, whereas peaks at 2,897 and 1,636 cm^{-1} were the stretching of the C–H group and the C=O carboxyl group, respectively. These results have been published in the study [21]. However, in the case of PEG-PEI-SWCNTs, as shown in Figure 5, the peak at 3,431 cm^{-1} shifted to 3,432 cm^{-1} and also the appearance of C–H at 2,883 cm^{-1}, which proved that SWCNTs are in conjunction with PEG-PEI. Additionally, the appearance of C=C at 1,468 cm^{-1} and C=O at 1,716 cm^{-1} was also identified, and the peaks at 1,616 and 1,344 cm^{-1} are related to N–H and C–N, respectively [28].

3.1.6. AFM Analysis. Figure 6 shows the AFM analysis of SWCNTs, and PEG-PEI-SWCNTs in SWCNTs image show a carbon nanotube with a grain size of 60 nm; these results have been published in a study [21]. Aggregation of SWCNTs with PEG 4000-PEI increases grain size with functionalization to 80.68 nm in PEG-PEI-SWCNTs.

3.2. Antiproliferative Activity of PEG-PEI-SWCNTs on Breast Cells. PEG-PEI-SWCNT's cytotoxicity evaluation against AMJ13 cells demonstrated increased cell toxicity with concentrations of 6.25–100 μg/mL (Figure 7). The results of the effect of SWCNTs on AMJ13 cells have been published in the study [21], and PEG-PEI-SWCNTs demonstrated 60% and 77.5% cytotoxicity at 100 μg/mL (Figure 7(a)). Apoptosis characterization was evaluated using structural modifications in the cells. The treated cells retained their original morphological form, as seen in the control cells. AMJ13 cell lines that were treated with PEG-PEI-SWCNTs exhibited morphological alterations. Figure 7(c) demonstrates decreased cytotoxicity owing to the decreased presence of cell colonies treated with PEG-PEI-SWCNTs, due to increased cytotoxicity [29, 30]. Structural changes, lack of communication with neighboring cells, and decreased number as concentration increases reflect a synergistic effect at higher doses, resulting in a greater impact than the lower dose [29]. The increased cytotoxicity observed with PEG-PEI-SWCNTs (Figure 7(b)) could be attributed to PEG grafting onto CNTs, which results in an efficient electrostatic layer of PEG's that increased SWCNT dispersion. The SWCNTs' antistatic potential helps in tackling gravitational and van der Waals forces leading to an extensive aqueous solution, resulting in increased aqueous dispersibility. Incorporating PEG into SWCNT's surface enhances biocompatibility, which may be responsible for PEG's nontoxic, nonantigenic, and distinctive physicochemical properties. Because of their increased positive charge NH_4^+ ion density, PEIs can improve bioavailability [31], resulting in chemical modification of the surface charge and cytotoxicity [32]. PEIs are used in coating materials for inorganic nanoparticles and gene delivery. They also reveal a crucial endosomal escape potential following intracellular absorption through the "proton sponge" effect [33] and neutral biocompatible polymers, as they prolong the drug release time and improve the killing effect on cells [34, 35].

3.3. Effect of PEG-PEI-SWCNTs on Normal Cells. The cytotoxic effect of PEG-PEI-SWCNTs on a normal cell line (RD) was studied to show the effectiveness of these substances in killing infected cells at a range of concentrations ranging between 6.26 and 100 μg/mL, as shown in Figure 8. These substances show a low percentage of killing activity for

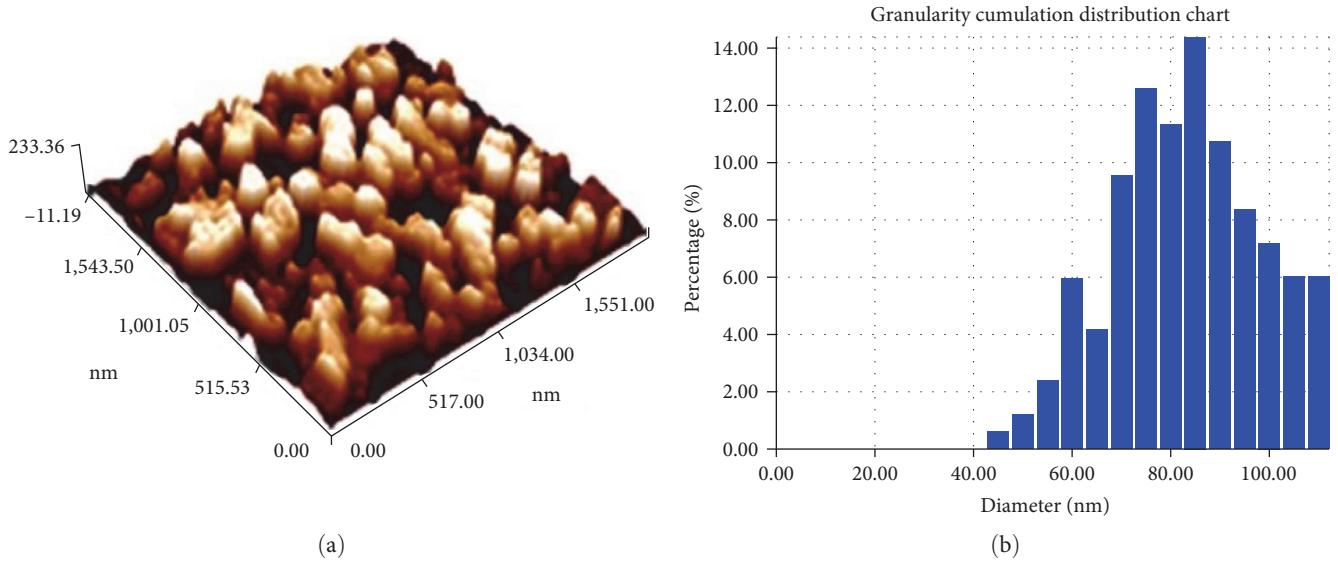

Figure 6: AFM topography analysis for PEG-PEI-SWCNTs: (a) surface image and (b) size distribution.

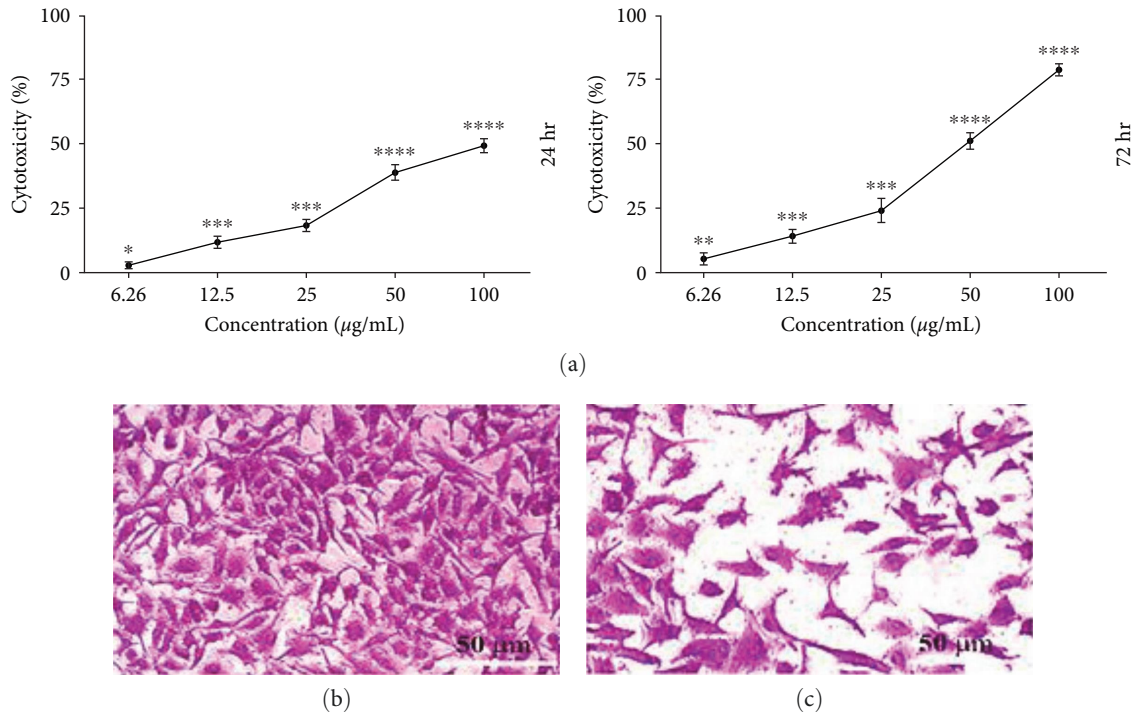

Figure 7: Cytotoxicity of PEG-PEI-SWCNTs against AMJ13 cells: (a) after 24 and 72 hr, respectively. Morphological changes were assessed for AMJ13 cells; (b) untreated cells; (c) treated cells with PEG-PEI-SWCNTs. Untreated cells were used to control for normalization. Data are represented as mean ± SD from three independent experiments. Asterisk (*) indicated a significant difference ($p < 0.05$), ** indicated a significant difference ($p < 0.01$), *** indicated a significant difference ($p < 0.001$), and **** indicated a significant difference ($p < 0.0001$). Scale bar: 50 μm.

the RD cells, with effectiveness increasing with increased concentration of the PEG-PEI-SWCNTs. We note that almost 13% of the RD cells was killed with a concentration of 100 μg/mL of PEG-PEI-SWCNTs.

The toxicity of MWCNTs was demonstrated by Santos et al. [36], with results showing that OH- and COOH-functionalized MWCNTs exert toxicity to both A549 and BEAS-2B cancer cells via various mechanisms with no toxic effects or significant damage to normal cells. In a similar work, a group of researchers tested the behavior of PEG-functionalized MWCNTs loaded with ABT-737, a nanodrug for treating lung cancer cells, against A549 cells. The findings showed 56% apoptosis for cancer cells, whereas normal cell apoptosis was reported to be 3% [37].

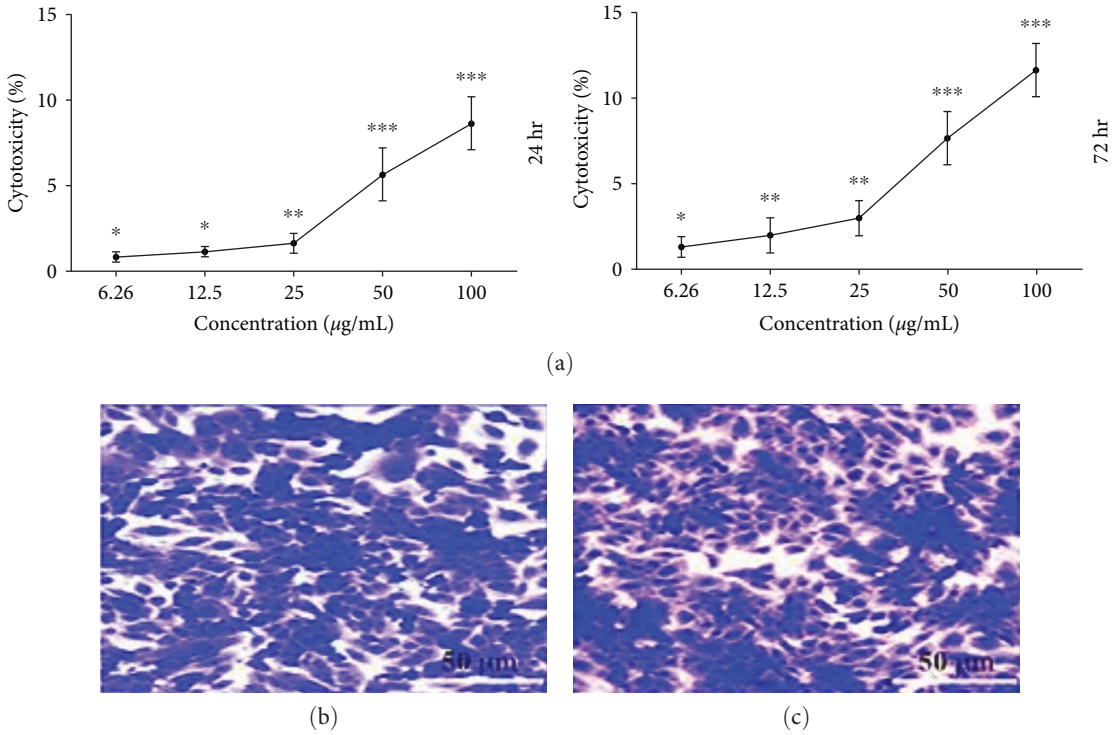

FIGURE 8: Cytotoxicity of PEG-PEI-SWCNTs against RD cells: (a) after 24 and 72 hr, respectively. Morphological changes were assessed for RD cells; (b) untreated cells; (c) treated cells with PEG-PEI-SWCNTs. Untreated cells were used to control for normalization. Data are represented as mean ± SD from three independent experiments. Asterisk (*) indicated a significant difference ($p < 0.05$), ** indicated a significant difference ($p < 0.01$), and *** indicated a significant difference ($p < 0.001$). Scale bar: 50 μm.

SWCNT-PEG-10-10%PEI NPs modified with AS1411 were used for delivering Bcl-xL short hairpin RNA (shRNA) and doxorubicin (DOX) to human gastric adenocarcinoma cell line (AGS) gastric cancer cells and L929 normal fibroblastic cells. The potential cytotoxic synergy of DOX and Bcl-xL shRNA toward AGS cells was evaluated using the MTT test and showed that the combination of pBcl-xL shRNA/SWCNT-PEG-10-10%PEI-Apt/DOX decreased cell viability of AGS cells which was 77%. Bcl-xL expression did not change in L929 cells treated with SWCNT-PEG-PEI-Apt/pBcl-xL shRNA assessing that the addition of AS1411 aptamer to nanoparticles could not enhance the Bcl-xL expression and, thus, the transfection efficiency, which is due to the absence of cell surface nucleolin on the surface of L929 cells [38].

4. Conclusion

PEG-containing SWCNTs and PEI-containing amines were described in this study. To improve aqueous solubility, the SWCNTs were first shortened using ultrasonic scissors in a variety of strong acids. The CNTs were then grafted using PEG and PEI. This functionalization was predicted to improve tumor site targeting while also reducing premature nanocarrier removal and loss. XRD, UV–vis spectroscopy, RS, AFM, FTIR, and TEM characterized the composite (PEG-PEI-SWCNTs). The results obtained in this study revealed enhanced cytotoxicity against AMJ13 cells and the effect was concentration dependent with less cytotoxicity against normal cells. Further, *in vivo* studies are now under investigation.

Data Availability

All the data are provided in the manuscript.

Conflicts of Interest

The authors declare that they have no conflicts of interest.

Authors' Contributions

M. R. Jwameer, S. A. Salman, and F. T. M. Noori conceptualized the study. M. R. Jwameer, S. A. Salman, F. T. M. Noori, G. M. Sulaiman, and M. S. Jabir contributed to methodology. S. A. Salman, K. A. A. Khalil, and M. T. A. Soliman took part in the formal analysis. F. T. M. Noori, M. S. Jabir, G. M. Sulaiman, K. A. A. Khalil, and M. T. A. Soliman investigated the study. M. R. Jwameer, S. A. Salman, and F. T. M. Noori provided resources. G. M. Sulaiman, M. S. Jabir, and M. T. A. Soliman were responsible for data curation. M. R. Jwameer, S. A. Salman, F. T. M. Noori, and M. S. Jabir prepared the original draft. G. M. Sulaiman, M. S. Jabir, and K. A. A. Khalil reviewed and edited the manuscript. S. A. Salman, G. M. Sulaiman, and M. S. Jabir supervised the study. G. M. Sulaiman and M. S. Jabir were responsible for project administration. K. A. A. Khalil, E. M. Ahmed, and M. T. A. Soliman

were responsible for funding acquisition. All authors have read and agreed to the published version of the manuscript.

Acknowledgments

The authors also thank their respective institutions for infrastructure support. The University of Diyala, the University of Baghdad, the University of Technology, Iraq, and the University of Bisha, Saudi Arabia, are thanked and gratefully acknowledged for their constant encouragement during the course of this study.

References

[1] Z. Liu, S. Tabakman, K. Welsher, and H. Dai, "Carbon nanotubes in biology and medicine: *in vitro* and *in vivo* detection, imaging and drug delivery," *Nano Research*, vol. 2, pp. 85–120, 2009.

[2] C. J. Gannon, P. Cherukuri, B. I. Yakobson et al., "Carbon nanotube-enhanced thermal destruction of cancer cells in a noninvasive radiofrequency field," *Cancer*, vol. 110, no. 12, pp. 2654–2665, 2007.

[3] F. Liang and B. Chen, "A review on biomedical applications of single-walled carbon nanotubes," *Current Medicinal Chemistry*, vol. 17, no. 1, pp. 10–24, 2010.

[4] M. Mahmood, A. Karmakar, A. Fejleh et al., "Synergistic enhancement of cancer therapy using a combination of carbon nanotubes and anti-tumor drug," *Nanomedicine*, vol. 4, no. 8, pp. 883–893, 2009.

[5] N. Kotagiri and J. W. Kim, "Stealth nanotubes: strategies of shielding carbon nanotubes to evade opsonization and improve biodistribution," *International Journal of Nanomedicine*, vol. 9, Supplement 1, pp. 85–105, 2014.

[6] A. von Harpe, H. Petersen, Y. Li, and T. Kissel, "Characterization of commercially available and synthesized polyethylenimines for gene delivery," *Journal of Controlled Release*, vol. 69, no. 2, pp. 309–322, 2000.

[7] H. Najafi, S. S. Abolmaali, B. Owrangi, Y. Ghasemi, and A. M. Tamaddon, "Serum resistant and enhanced transfection of plasmid DNA by PEG-stabilized polyplex nanoparticles of L-histidine substituted polyethyleneimine," *Macromolecular Research*, vol. 23, pp. 618–627, 2015.

[8] G. P. Tang, J. M. Zeng, S. J. Gao et al., "Polyethylene glycol modified polyethylenimine for improved CNS gene transfer: effects of PEGylation extent," *Biomaterials*, vol. 24, no. 13, pp. 2351–2362, 2003.

[9] H. A. Mohammed, S. A. Almahmoud, E.-S. M. El-Ghaly et al., "Comparative anticancer potentials of taxifolin and quercetin methylated derivatives against HCT-116 cell lines: effects of *O*-methylation on taxifolin and quercetin as preliminary natural leads," *ACS Omega*, vol. 7, pp. 46629–46639, 2022.

[10] B. Sun, N. Hu, L. Han, Y. Pi, Y. Gao, and K. Chen, "Anticancer activity of green synthesised gold nanoparticles from *Marsdenia tenacissima* inhibits A549 cell proliferation through the apoptotic pathway," *Artificial Cells, Nanomedicine, and Biotechnology*, vol. 47, no. 1, pp. 4012–4019, 2019.

[11] N. E.-A. El-Naggar, M. H. Hussein, and A. A. El-Sawah, "Bio-fabrication of silver nanoparticles by phycocyanin, characterization, *in vitro* anticancer activity against breast cancer cell line and *in vivo* cytotxicity," *Scientific Reports*, vol. 7, Article ID 10844, 2017.

[12] H. M. Abd-Elhady, M. A. Ashor, A. Hazem et al., "Biosynthesis and characterization of extracellular silver nanoparticles from *Streptomyces aizuneusis*: antimicrobial, anti larval, and anticancer activities," *Molecules*, vol. 27, no. 1, Article ID 212, 2021.

[13] H. Singh, J. Du, P. Singh, and T. H. Yi, "Ecofriendly synthesis of silver and gold nanoparticles by *Euphrasia officinalis* leaf extract and its biomedical applications," *Artificial Cells, Nanomedicine, and Biotechnology*, vol. 46, no. 6, pp. 1163–1170, 2018.

[14] S. Dinparvar, M. Bagirova, A. M. Allahverdiyev et al., "A nanotechnology-based new approach in the treatment of breast cancer: biosynthesized silver nanoparticles using *Cuminum cyminum* L. seed extract," *Journal of Photochemistry and Photobiology B: Biology*, vol. 208, Article ID 111902, 2020.

[15] S. Elhawary, H. El-Hefnawy, F. A. Mokhtar et al., "Green synthesis of silver nanoparticles using extract of *Jasminum officinal* L. leaves and evaluation of cytotoxic activity towards bladder (5637) and breast cancer (MCF-7) cell lines," *International Journal of Nanomedicine*, vol. 15, pp. 9771–9781, 2020.

[16] H. Padalia and S. Chanda, "Synthesis of silver nanoparticles using *Ziziphus nummularia* leaf extract and evaluation of their antimicrobial, antioxidant, cytotoxic and genotoxic potential (4-in-1 system)," *Artificial Cells, Nanomedicine, and Biotechnology*, vol. 49, no. 1, pp. 354–366, 2021.

[17] M. Buttacavoli, N. N. Albanese, G. Di Cara et al., "Anticancer activity of biogenerated silver nanoparticles: an integrated proteomic investigation," *Oncotarget*, vol. 9, pp. 9685–9705, 2018.

[18] E. S. Al-Sheddi, N. N. Farshori, M. M. Al-Oqail et al., "Anticancer potential of green synthesized silver nanoparticles using extract of *Nepeta deflersiana* against human cervical cancer cells (HeLA)," *Bioinorganic Chemistry and Applications*, vol. 2018, Article ID 9390784, 12 pages, 2018.

[19] A. M. Sameen, M. S. Jabir, and M. Q. Al-Ani, "Therapeutic combination of gold nanoparticles and LPS as cytotoxic and apoptosis inducer in breast cancer cells," *AIP Conference Proceedings*, vol. 2213, no. 1, Article ID 020215, 2020.

[20] H. H. Bahjat, R. A. Ismail, G. M. Sulaiman, and M. S. Jabir, "Magnetic field-assisted laser ablation of titanium dioxide nanoparticles in water for anti-bacterial applications," *Journal of Inorganic and Organometallic Polymers and Materials*, vol. 31, pp. 3649–3656, 2021.

[21] M. R. Jwameer, F. T. M. Noori, and S. A. Anwer, "Carbon nanotube conjugate with PEG as a drug delivery in to AMJ13 and HepG2 cell," *Journal of Mechanical Engineering Research and Development*, vol. 44, no. 10, pp. 44–56, 2021.

[22] S. Yang, Z. Wang, Y. Ping et al., "PEG/PEI-functionalized single-walled carbon nanotubes as delivery carriers for doxorubicin: synthesis, characterization, and in vitro evaluation," *Beilstein Journal of Nanotechnology*, vol. 11, pp. 1728–1741, 2020.

[23] A. B. Leite, C. Saucier, E. C. Lima et al., "Activated carbons from avocado seed: optimisation and application for removal of several emerging organic compounds," *Environmental Science and Pollution Research*, vol. 25, pp. 7647–7661, 2018.

[24] D. Ravelli, D. Merli, E. Quartarone, A. Profumo, P. Mustarelli, and M. Fagnoni, "PEGylated carbon nanotubes: preparation, properties and applications," *RSC Advances*, vol. 3, no. 33, pp. 13569–13582, 2013.

[25] Y. Sun and Z. Li, "Aqueous dispersion of single walled carbon nanotubes stabilized by PEG modified diperylene bisimide and their application as an antibacterial agent," *RSC Advances*, vol. 7, no. 42, pp. 26125–26129, 2017.

[26] A. Jorio, R. Saito, J. H. Hafner et al., "Structural (n, m) determination of isolated single-wall carbon nanotubes by resonant Raman scattering," *Physical Review Letters*, vol. 86, no. 6, pp. 1118–1121, 2001.

[27] S. Kumar, V. Pavelyev, P. Mishra, and N. Tripathi, "Thin film chemiresistive gas sensor on single-walled carbon nanotubes-functionalized with polyethylenimine (PEI) for NO_2 gas sensing," *Bulletin of Materials Science*, vol. 43, Article ID 61, 2020.

[28] S. Roy, L. Van Hai, and J. Kim, "Synergistic effect of polydopamine–polyethylenimine copolymer coating on graphene oxide for EVA nanocomposites and high-performance triboelectric nanogenerators," *Nanoscale Advances*, vol. 1, no. 6, pp. 2444–2453, 2019.

[29] Q. Zhang, F. Yu, M. Lei, H. Fu, G. Yan, and L. Li, "Synthesis, characterization, and evaluation of disulfide-containing polyethylenimine derivative functionalized magnetic carbon nanotubes as an efficient gene vector," *Journal of Nanomaterials*, vol. 2019, Article ID 6026390, 11 pages, 2019.

[30] M. Abdullah, F. T. Mohammed Noori, and A. H. Al-Khursan, "Terahertz emission in ladder plus Y-configurations in double quantum dot structure," *Applied Optics*, vol. 54, no. 16, pp. 5186–5192, 2015.

[31] L. Amigo and B. Hernández-Ledesma, "Current evidence on the bioavailability of food bioactive peptides," *Molecules*, vol. 25, no. 19, Article ID 4479, 2020.

[32] H. M. Hasan, "A study of the structural and electrical properties of Ni_{1-x} Cox Fe_2O_4 ferrites," *Iraqi Journal of Physics*, vol. 12, no. 25, pp. 69–79, 2014.

[33] S. Yu, Y. Zhang, L. Chen et al., "Antitumor effects of carbon nanotube-drug complex against human breast cancer cells," *Experimental and Therapeutic Medicine*, vol. 16, no. 2, pp. 1103–1110, 2018.

[34] M. Shen, S. H. Wang, X. Shi et al., "Polyethyleneimine-mediated functionalization of multiwalled carbon nanotubes: synthesis, characterization, and in vitro toxicity assay," *The Journal of Physical Chemistry C*, vol. 113, no. 8, pp. 3150–3156, 2009.

[35] J. Heller, "Biodegradable polymers in controlled drug delivery," *Critical Reviews in Therapeutic Drug Carrier Systems*, vol. 1, no. 1, pp. 39–90, 1984.

[36] T. Santos, X. Fang, M.-T. Chen et al., "Sequential administration of carbon nanotubes and near-infrared radiation for the treatment of gliomas," *Frontiers in Oncology*, vol. 4, Article ID 180, 2014.

[37] H. Zare, S. Ahmadi, A. Ghasemi et al., "Carbon nanotubes: smart drug/gene delivery carriers," *International Journal of Nanomedicine*, vol. 16, pp. 1681–1706, 2021.

[38] B. Ferrara, S. Belbekhouche, D. Habert et al., "Cell surface nucleolin as active bait for nanomedicine in cancer therapy: a promising option," *Nanotechnology*, vol. 32, no. 32, Article ID 322001, 2021.